POLITECNICO DI TORINO
Repository ISTITUZIONALE

ChatGPT, be my teaching assistant! Automatic correction of SQL exercises

Original
ChatGPT, be my teaching assistant! Automatic correction of SQL exercises / Cagliero, L., Farinetti, L., Fior, J., Manenti, A.I.. - STAMPA. - (2024), pp. 81-87. (2024 IEEE 48th Annual Computers, Software, and Applications Conference (COMPSAC) Osaka (JPN) July 2-4, 2024) [10.1109/COMPSAC61105.2024.00021].

Availability:
This version is available at: 11583/2995636 since: 2024-12-19T08:28:30Z

Publisher:
979-8-3503-7696-8

Published
DOI:10.1109/COMPSAC61105.2024.00021

Terms of use:

This article is made available under terms and conditions as specified in the corresponding bibliographic description in the repository

Publisher copyright
IEEE postprint/Author's Accepted Manuscript

©2024 IEEE. Personal use of this material is permitted. Permission from IEEE must be obtained for all other uses, in any current or future media, including reprinting/republishing this material for advertising or promotional purposes, creating new collecting works, for resale or lists, or reuse of any copyrighted component of this work in other works.

(Article begins on next page)

15 November 2026

Nuclear Engineering and Technology xxx (xxxx) xxx

Contents lists available at ScienceDirect

Nuclear Engineering and Technology

journal homepage: www.elsevier.com/locate/net

Original Article

Benchmark of system thermal-hydraulic codes for the test section of the dip cooler instability test facility

Danilo Caterino [a,*], Giuseppe Spina [b], Roberto Bonifetto [a], Antonino Lombardo [b], Fabio Moretti [b], Giuseppe Francesco Nallo [b], Valeria Parrinello [b], Matteo Rostagno [b], Raffaella Testoni [a]

[a] Politecnico di Torino, Energy Department "Galileo Ferraris", Corso Duca degli Abruzzi 24, 10129, Torino, Italy
[b] Newcleo S.p.A., via Giuseppe Galliano 27, 10129, Torino, Italy

ARTICLE INFO

Keywords:
Lead-cooled fast reactors
Decay heat removal
Bayonet tubes
Low pressure operation
ATHLET
RELAP

ABSTRACT

The Dip Cooler Instability (DCI) Test Facility is designed to investigate the thermal-hydraulic behavior of two parallel bayonet tubes, and aims at supporting the characterization of the dip cooler Decay Heat Removal (DHR) system employed in *new*cleo's 30 MWe Amphora-Shaped Lead-cooled Fast Reactor (LFR-AS-30).

Within the framework of *new*cleo's Verification and Validation (V&V) roadmap, this study presents a code-to-code benchmark based on the pre-test model developed with the system thermal-hydraulic codes AC^2-ATHLET 3.4.1 and RELAP/SCDAPSIM/MOD4.1.

Focusing on a subset of cases in the experimental test matrix, the numerical results are compared to assess the level of agreement between the codes. The comparison highlights significant differences mainly stemming from the determination of the heat transfer mode and from the interphase mass transfer model.

Then, the comparison with the experiments reveals discrepancies caused by the deviation of the measured wall temperature from the setpoint, as well as by a possible underestimation of the effective thermal conductivity of the helium gap in the numerical models. This consideration is corroborated by a preliminary uncertainty quantification analysis performed with the ATHLET code. Future activities will focus on the post-test analyses performed with a more detailed model of the DCI Test Facility.

1. Introduction

Lead-cooled Fast Reactors (LFRs) are considered among the most promising next-generation nuclear technologies due to their enhanced safety and sustainability features [1]- [2]- [3]. This vision is shared by *new*cleo and represents the foundation of the design of a 30 MWe first-of-a-kind Amphora-Shaped LFR (LFR-AS-30), planned for 2031 [4]. A conceptual sketch of the LFR-AS-30 is presented in Fig. 1a.

Decay Heat Removal (DHR) systems play a crucial role in ensuring reactor safety during shutdown scenarios. The primary DHR system (DHR-1) employed in the LFR-AS-30 is based on a dip cooler design, consisting of multiple bundles of bayonet tubes immersed in the reactor primary coolant. A conceptual scheme of a single bayonet tube is reported in Fig. 1b. The use of bayonet tubes has been also conceptualized for the steam generator (serving also as DHR) of the ALFRED reactor [5]-[6]. One of the options presently being investigated for the DHR-1 of the LFR-AS-30 consists in a passive system operating at atmospheric pressure: water is driven by gravity from a reservoir (positioned at an appropriate height) toward each dip cooler heat exchanger.

Within each bayonet tube, the coolant flows downward through the downcomer (i.e., inside the inner tube) and then upward within the riser (i.e., in the annular gap between the inner and intermediate tube), where it reaches saturation conditions. Regenerative heat transfer may occur between the downcomer and the riser, especially if the inner tube is not insulated. The gap between the intermediate and outer tubes is filled with pressurized helium, enabling a prompt detection of possible ruptures. The design of passive systems requires a thorough thermal-hydraulic investigation from both the experimental and numerical

* Corresponding author.
E-mail addresses: danilo.caterino@polito.it (D. Caterino), giuseppe.spina@newcleo.com (G. Spina), roberto.bonifetto@polito.it (R. Bonifetto), antonino.lombardo.2@newcleo.com (A. Lombardo), fabio.moretti@newcleo.com (F. Moretti), giuseppe.nallo@newcleo.com (G.F. Nallo), valeria.parrinello@newcleo.com (V. Parrinello), matteo.rostagno@newcleo.com (M. Rostagno), raffaella.testoni@polito.it (R. Testoni).

https://doi.org/10.1016/j.net.2026.104387
Received 10 January 2026; Received in revised form 23 March 2026; Accepted 25 April 2026
Available online 27 April 2026
1738-5733/© 2026 Korean Nuclear Society, Published by Elsevier Korea LLC. This is an open access article under the CC BY license (http://creativecommons.org/licenses/by/4.0/).

point of view [7]. Moreover, one of the phenomena to be characterized is the potential onset of two-phase flow instabilities [8].

Experimental facilities dedicated to passive bayonet-type DHR systems included: PROPHET, operated at Politecnico di Torino (now decommissioned) to investigate the thermal–hydraulic behavior of a single bayonet tube of the ALFRED DHR-2 [9]; SIRIO, operated by ENEA to test the ALFRED DHR system using a bayonet tube bundle and a passive power regulation mechanism based on non-condensable gas concentration [10]; the coupled HEXACOM and COMPLOT facilities at SCK-CEN which aimed at investigating the thermal-hydraulic behavior of a single double-wall bayonet tube immersed in LBE and reproduced from the MYRRHA primary heat exchanger serving also as DHR system [11]; CIRCE LBE integral facility at the ENEA Brasimone Research Centre, equipped with the HERO test section, which included a bayonet tube bundle for the heat removal [12]; and the HERO-2 facility operated by ENEA to investigate the behavior of two bayonet tubes at high pressure [13].

Although many experimental facilities dedicated to bayonet tube heat exchangers are available, the thermal-hydraulic performance and instability characteristics of the LFR-AS-30 DHR-1 system under passive operation and atmospheric pressure still require dedicated investigation. To this aim, *new*cleo is deploying an extensive experimental programme aiming at investigating specific phenomena, qualifying components and validating scientific computing tools. Overall, this programme encompasses both Separate Effect Test Facilities (SETFs) and Integral Test Facilities (ITFs), including Precursor, a 1:9 scaled ITF designed to be representative of the LFR-AS-30 design. In this framework, the Dip Cooler Instability (DCI) Test Facility has been designed to fill the gap identified into the characterization thermal-hydraulic behavior of the LFR-AS-30 DHR-1 system.

This work aims at supporting *new*cleo's experimental programme on the DHR-1 focusing on the pre-test analyses of the DCI Test Facility. Specifically, a code-to-code benchmark between the two system thermal-hydraulic codes AC^2-ATHLET 3.4.1 [14] and RELAP/SCDAPSIM/MOD4.1 [15] is proposed in order to highlight the main differences stemming from the implemented numerical models. Then, a preliminary code-to-experiment comparison is presented in order to critically investigate the discrepancies between the yielded numerical results and the experiments. Some of the considerations drawn from the discrepancies between the experiments and the codes are supported by a preliminary uncertainty quantification activity performed with the ATHLET code.

2. The DCI test facility

The Dip Cooler Instability (DCI) Test Facility, designed and built by *new*cleo, is located within the Energy Department of Politecnico di Torino. It consists of a water tank, a feedwater pipeline, a test section and a steam pipeline. A schematic of the setup, as well as pictures of the key components, are shown in Fig. 2. A simplified PI&D is presented in Fig. 3, and the operating conditions are summarized in Table 1. The experimental data presented in this work are acquired at a sampling frequency of 2 Hz. However, provisions have been made to enable higher sampling rates and the installation of high-frequency sensors for the analysis of two-phase flow instabilities.

2.1. General overview

The water tank, shown in Fig. 2b, is positioned at a sufficient height (approximately 7 m from the test section) to ensure enough gravity head (approximately 0.7 barg) to drive the desired water flow rate. A level sensor (LS in Fig. 3) constantly monitors the available water inventory within the tank. To further expand the scope of the experimental investigations, the tank can be pressurized with nitrogen or air through a dedicated pneumatic circuit. The pressure and the temperature sensors (PS-1 and TC-1 in Fig. 3) provide information about the internal condition of the tank. The desired mass flow rate is achieved by using a PID-controlled valve located along the feedwater line, near the inlet of the test section (see Figs. 2b and 3). With reference to Fig. 3, a Coriolis-type sensor (FT) measures the mass flow rate within the feedwater line. The line is also equipped with a pressure sensor before the feedwater valve (PS-2) and a thermocouple downstream of the valve (TC-2).

The steam pipeline redirects the two-phase mixture flowing out of the test section toward the environment. As illustrated in Fig. 3, the steam pipeline is equipped with a pressure and a temperature sensor (PS-3 and TC-3, respectively). Condensed water is removed by a ball float steam trap placed along the line (as in Fig. 3), while generated steam is released into the environment thanks to a dedicated chimney.

A first experimental campaign has been carried out according to the test matrix which covers three types of tests:

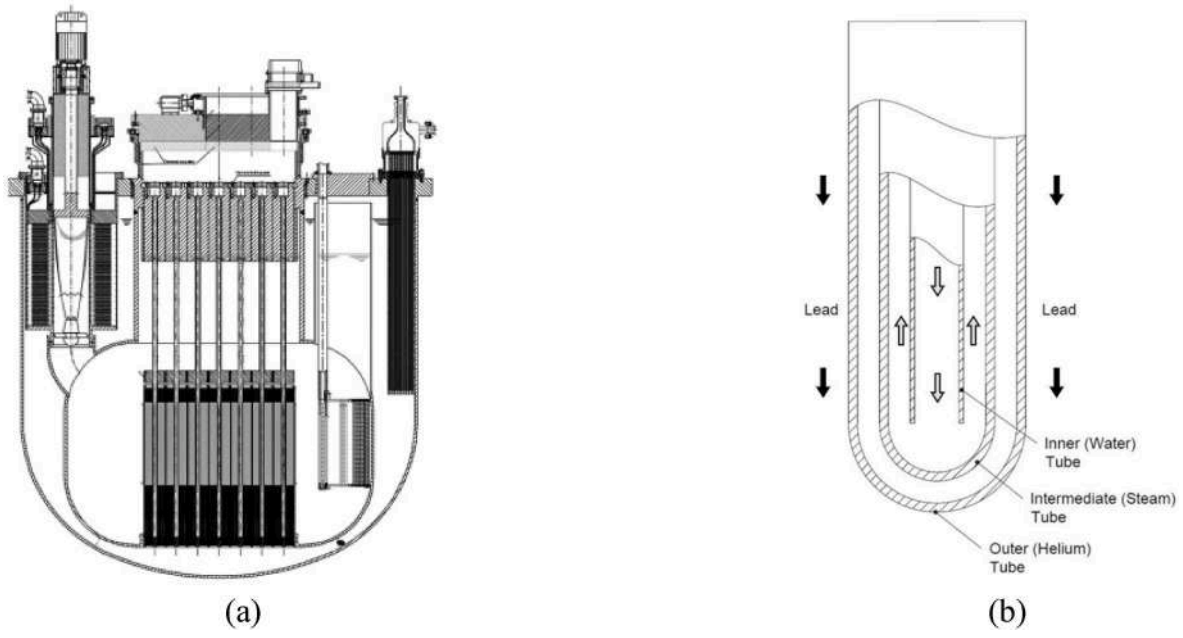


Fig. 1. Conceptual representation of *new*cleo's LFR-AS-30 reproduced from Ref. [16] (1a); conceptual representation of a single bayonet tube (1b).

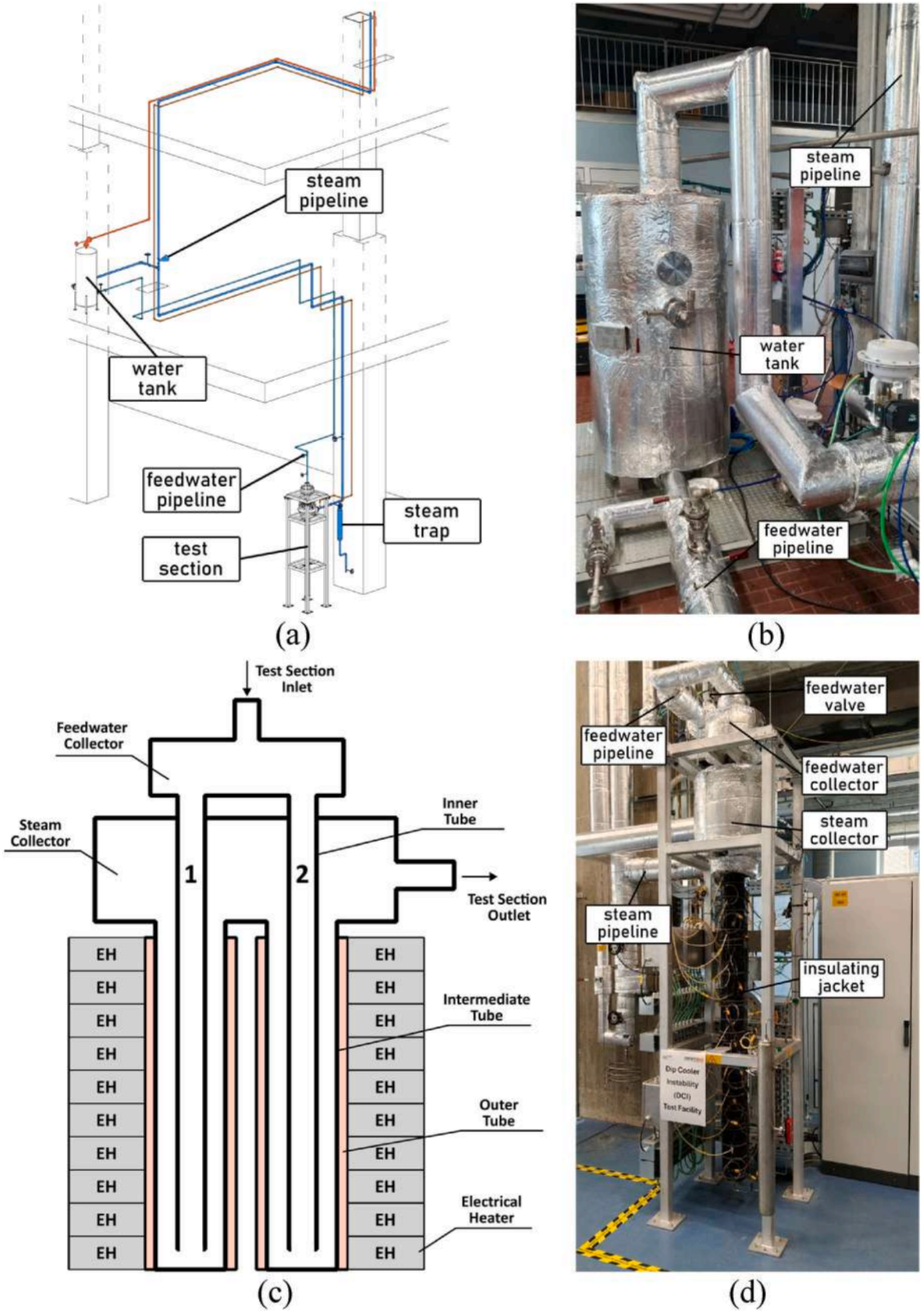


Fig. 2. The DCI Test Facility. Namely, the conceptual scheme of the facility (a), the water tank (b), the test section scheme (c), and the test section view (d).

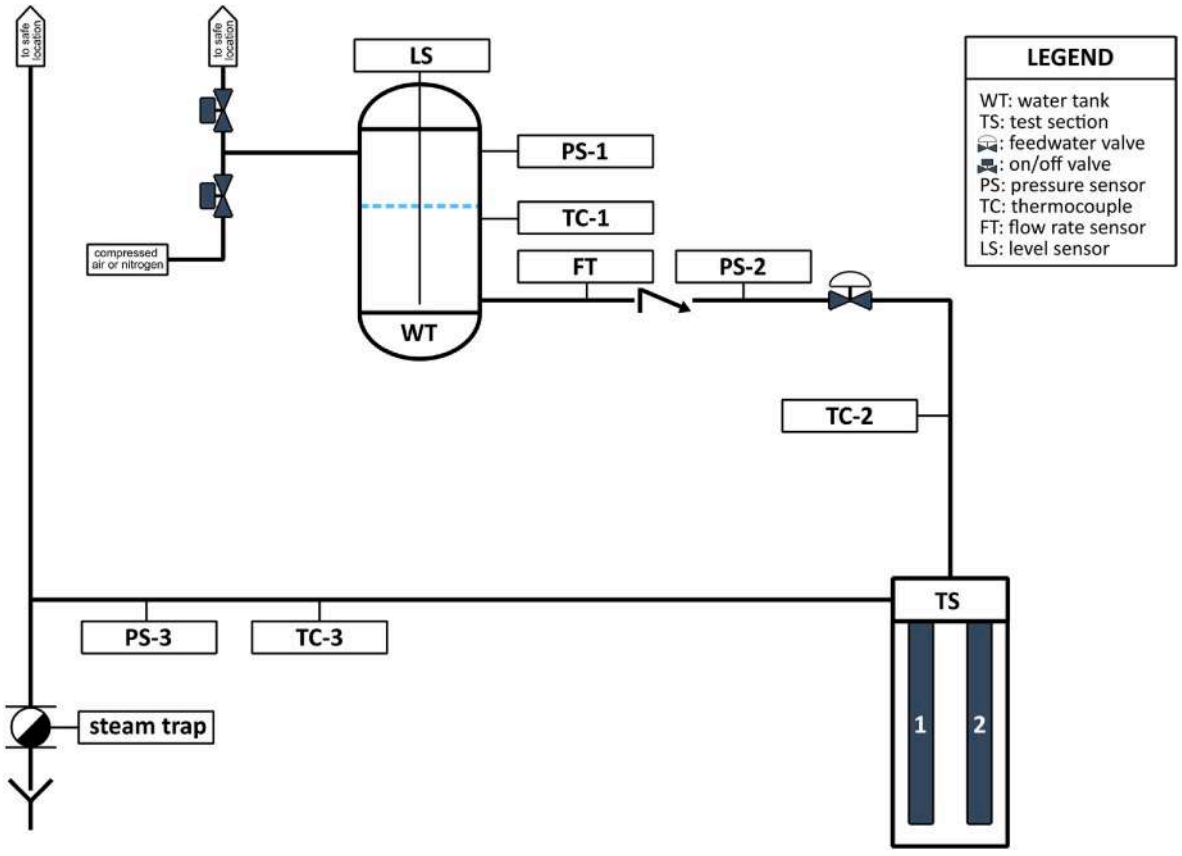


Fig. 3. Simplified P&ID of the DCI test facility.

Table 1
General operating conditions of the DCI Test Facility.

	Min	Max
Pressure (bar)	1	20
Temperature (°C)	20	650
Mass Flow Rate (g/s)	3.5	10

- A: characterization of heat losses toward the environment;
- B: characterization of steady-state behavior;
- C: characterization of the start-up phase of the DHR-1.

The activity discussed in this work focuses on the test section at steady-state (i.e. during tests of type B) at a system pressure of 1 bar.

2.2. Test section

The test section, shown in Fig. 2c and d, consists of a feedwater collector, two parallel bayonet tubes (of the type presented in Fig. 1b) and a steam collector. The two bayonet tubes are made of AISI 316 stainless steel, with their indicative inner and outer diameters reported in Table 2.

Under normal operating conditions, subcooled water flows downward from the feedwater collector towards the two inner tubes (with a length of 2.6 m each). An initial portion of the inner tubes runs across the steam collector as illustrated in Fig. 2c. The regenerative heat transfer between the steam collector and the inner tube causes preheating of the coolant. As the flow reaches the bottom of each inner tube, it turns upwards through the intermediate tube (having a length of 2.1 m), where saturated conditions are typically achieved. The two-phase mixture flows upward and, depending on the operating conditions, saturated or superheated steam reaches the steam collector. Regenerative heat transfer also occurs between the intermediate and inner tube as shown in Fig. 2c.

Table 2
Indicative diameters of the bayonet tube.

	Inner Diameter (mm)	Outer Diameter (mm)
Inner Tube	2	6
Intermediate Tube	11	14
Outer Tube	15	20

A uniform external temperature is applied to each bayonet tube using ten PID-driven electrical heaters, coiled around the outer tube as illustrated in the scheme in Fig. 2c. The nominal power of each heater is 923 W.

The heated length extends for 1.9 m, and is covered with an insulating jacket (see Fig. 2d) to reduce heat losses toward the surrounding environment. Each bayonet tube features also an outer tube filled with pressurized helium. Concentric alignment between the outer and intermediate tubes is ensured by metallic spacers uniformly distributed along the bayonet tube.

3. Numerical model

This section describes the pre-test numerical model of the DCI Test Facility developed using the system thermal-hydraulic codes AC^2-ATHLET 3.4.1 and RELAP/SCDAPSIM/MOD4.1.

The modeling approach used in the pre-test analysis embodies simplifications (especially in the application of the boundary conditions) designed to reduce complexity while maintaining an acceptable representativity of the facility. In both codes a two-phase equation system (6 equations model) is resolved and a total of 3600 s are simulated.

3.1. Nodalization

The following nodalization has been chosen after a sensitivity analysis to enhance numerical stability and minimize the required elapsed time (further details are presented in Appendix A).

With reference to Fig. 4a, the considered feedwater pipeline (fwline4) starts from the location of the feedwater valve. The feedwater collector, or plenum (DC.PL), at the entrance of the test section is represented with a branch. Each bayonet tube is modeled with two pipes – downcomer (DC) and riser (RS) for tube 1 and tube 2 – while the steam collector, or plenum (RS.PL) is represented with a branch. Flow inversion is allowed thanks to the tube plena at the bottom of the bayonet modeled as branches (PL.1 and PL.2). Three types of heat structures are used, namely:

1. The wall coupling each inner tube on the left (or inner) side and the steam collector on the right (or outer) side (DC.1.W and DC.2.W) to model the regenerative heat transfer;
2. The wall coupling each inner tube on the left (or inner) side and its respective intermediate tube on the right (or outer) side (DC.RS.1.W and DC.RS.2.W) to model the regenerative heat transfer;
3. The heated wall coupled with each intermediate tube on the left (or inner) side (RS.1.W and RS.2.W); the helium gap in the wall is modeled as a purely conductive layer.

The steam pipeline in Fig. 4b is represented by four pipes (sline1, sline2.in, sline2, sline3). Condensed water is drained by gravity and collected in a pipe (wtcoll) located between sline2.in and sline2. However, as mentioned above, the facility features a ball float steam trap, used to separate and release condensate. The remaining steamline separations are used to account for the presence of additional valves. These additional valves are modeled just as localized pressure losses since they are not utilized during normal operations, hence always open. Finally, a time-dependent volume (sline.tdv) is used at the end of the steamline, where the chimney for the steam release is located.

3.2. Boundary conditions

In the experimental setup, the PID control logic regulates the valve opening to achieve the desired mass flow rate. Rather than explicitly modelling the PID logic, during the pre-test analyses the mass flow rate is imposed as an inlet boundary condition, and the inlet temperature is set to a fixed value of 20.0 °C. In ATHLET, such conditions are enforced using a FILL object, whereas in RELAP a time-dependent volume and a time-dependent junction are used. The wall temperature is fixed to a prescribed value and is applied to the outer (or right) side of each heat structure representing the outer tube (i.e. Dirichlet boundary condition). Therefore, the PID logic controlling the power supplied by each heater based on the difference between the wall temperature and the setpoint has not been included in the presented numerical models. Outlet pressure is set to atmospheric thanks to the time-dependent volume located at the end of the steam pipeline.

3.3. Initial conditions

The feedwater pipeline, collector and both downcomers are initially filled with stagnant subcooled water (zero velocity). Conversely, both risers, the steam collector and the steam pipeline are initialized with stagnant steam (also at zero velocity). Specifically, the two-phase system is initialized at 1 bar, with the liquid phase at the inlet temperature (i.e. 20 °C), and the vapor phase at around 130 °C. The initial external wall temperature is set to 130 °C as well. It should be noticed that such initial conditions are not intended to replicate the test procedure adopted for the DCI Test Facility. Instead, they serve as a means to quickly and stably achieve the steady state of the system.

3.4. Test cases

The cases analyzed in this work (listed in Table 3) aim at investigating the effect of the mass flow rate at a wall temperature of 350 °C. The selected mass flow rate values are consistent with those explored during the experimental campaign. However, the lowest mass flow rate investigated experimentally (i.e. 3.5 g/s) is not included in the present analysis, as it may lead to flow instabilities (as observed in the

Table 3
List of simulated cases.

Case #	Feedwater mass flow rate (g/s)
01	10
02	8
03	6
04	5
05	4.5
06	4

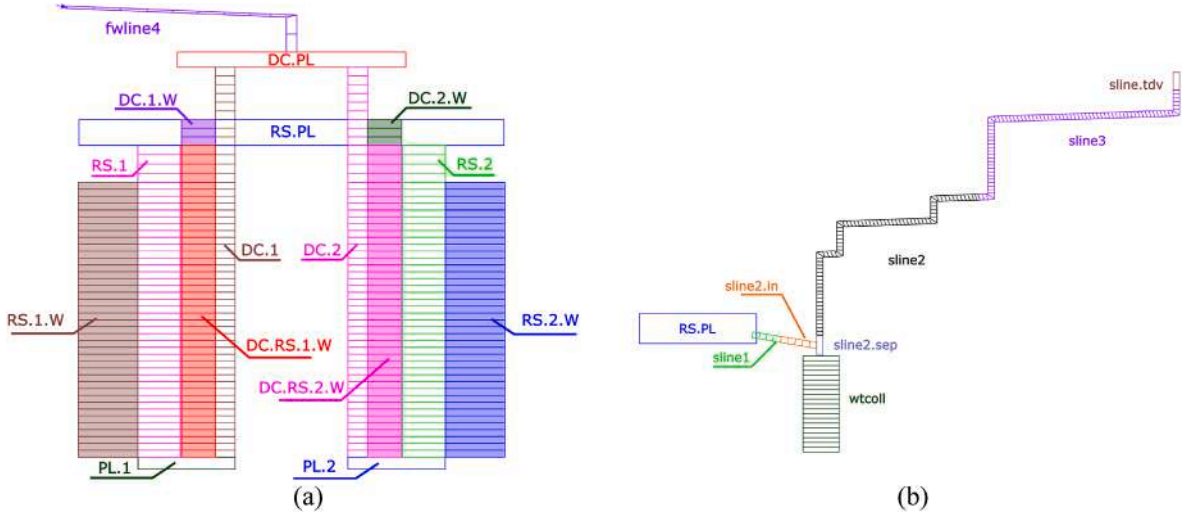


Fig. 4. Schematic (not to scale) of the adopted nodalization, representative of both AC^2-ATHLET 3.4.1 and RELAP/SCDAPSIM/MOD4.1 models. Namely, the simulated feedwater line and test section (a), and the steam pipeline (b). Unfilled boxes represent hydraulic components, whereas shaded boxes represent solid structures.

experiments). The investigation of this unstable regime is beyond the scope of the proposed work and will be addressed in future studies. The value of the wall temperature (i.e. 350 °C) is chosen because its corresponding experimental setpoint is achieved more consistently and uniformly along the tubes (as discussed later in this work) compared to higher setpoints. Thus, the selected value of the wall temperature is more representative of steady operation of the test section.

4. Main results and discussion

The analysis in this section proposes a code-to-code comparison of the time-averaged numerical results within the two bayonet tubes in a time frame between 3000 s and 3600 s. The standard deviation of the numerical results, intended to provide a quantification of the oscillations within the time span considered for the averaging, is also represented with bands colored with the respective tube and code color. Fig. 5 shows that, for some of the selected operating conditions (e.g. Fig. 5a for 10 g/s), the numerical results are substantially stable and display a relatively small standard deviation. Thus, although represented in Figs. 6–9, the band size may appear almost negligible compared to the marker size of the respective time-averaged value.

Additionally, some of the numerical cases discussed reveal a symmetric behavior of the tubes. Only in these cases, the numerical results yielded by the same code for the two tubes tend to perfectly overlap. Nevertheless, the numerical results for both tubes are shown to provide evidence of the observed symmetry.

The analysis then compares the computed total power and power distribution against the experimental results, discussing possible limitations of the adopted modelling approach.

Finally, a preliminary uncertainty quantification analysis has been conducted with the modified ATHLET model to evaluate the influence of some key parameters on the computed extracted power and power distribution.

4.1. Code-to-code comparison

The time-averaged numerical results in Fig. 6 highlight the nearly symmetric condition computed within the test section, as demonstrated by the overlapping lines belonging to the two tubes. Although the curves almost coincide, both sets of data are intentionally plotted to explicitly demonstrate the symmetry of the solution and to confirm that the behavior in the test section is virtually identical. However, decreasing the mass flow rate causes the test section to deviate from this symmetric condition, as suggested by the increasing standard deviation in Figs. 7 and 8 as opposed to Fig. 6, as well as by the more noticeable differences in the average results belonging to the same code.

Generally, ATHLET predicts the onset of the nucleate boiling regime slightly before the flow inversions, as demonstrated by the increase in the void fraction (Figs. 6b and 7b) and in total vapor generation (see Figs. 6e and 7e). As a result, the pressure distribution (Figs. 6a and 7a) is significantly different between the two codes.

Differences in the aforementioned quantities can be attributed to the interphase heat and mass transfer model implemented in ATHLET, specifically, to the reduction of the evaporation rate in the near-wall region (Figs. 6f and 7f) enforced by ATHLET when the operating pressure is below 10 bar.

Another key difference stemming from the ATHLET interphase heat and mass transfer can be observed in the temperature of the phases (reported in Fig. 6c, d, 7c and 7d). As a result of the reduced the near-wall evaporation model, ATHLET predicts a liquid temperature significantly above saturation. Moreover, as opposed to RELAP, the vapor temperature can be also significantly above saturation, even before wall dryout occurs.

The different implementation of the heat transfer modes can be another major source of discrepancy between the codes. Both codes rely on the same correlations (Dittus-Boelter for subcooled water [17] and Chen for nucleate boiling [18]) and use the same physical parameters (e.

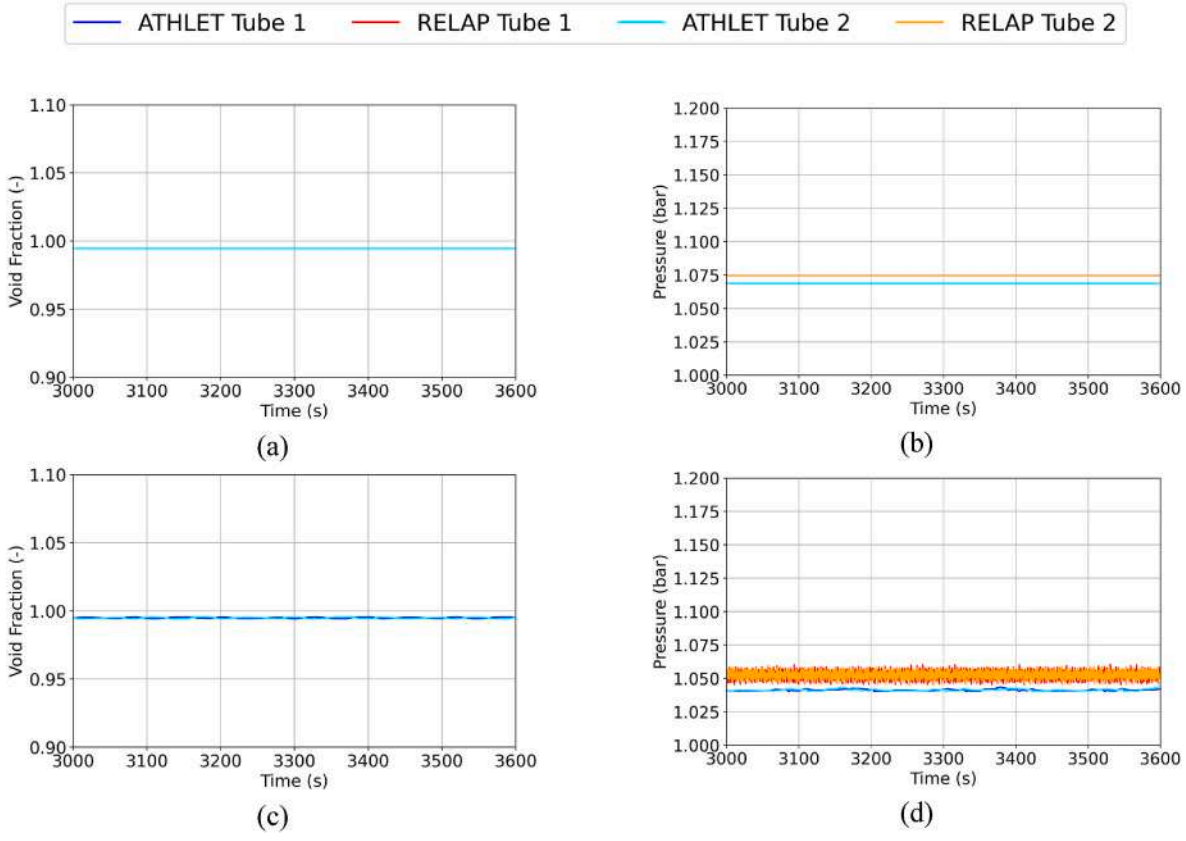


Fig. 5. Evolution of void fraction (left) and pressure (right) within each intermediate tube at the end of the heated length for Case01 (a)-(b), and Case03 (c)-(d).

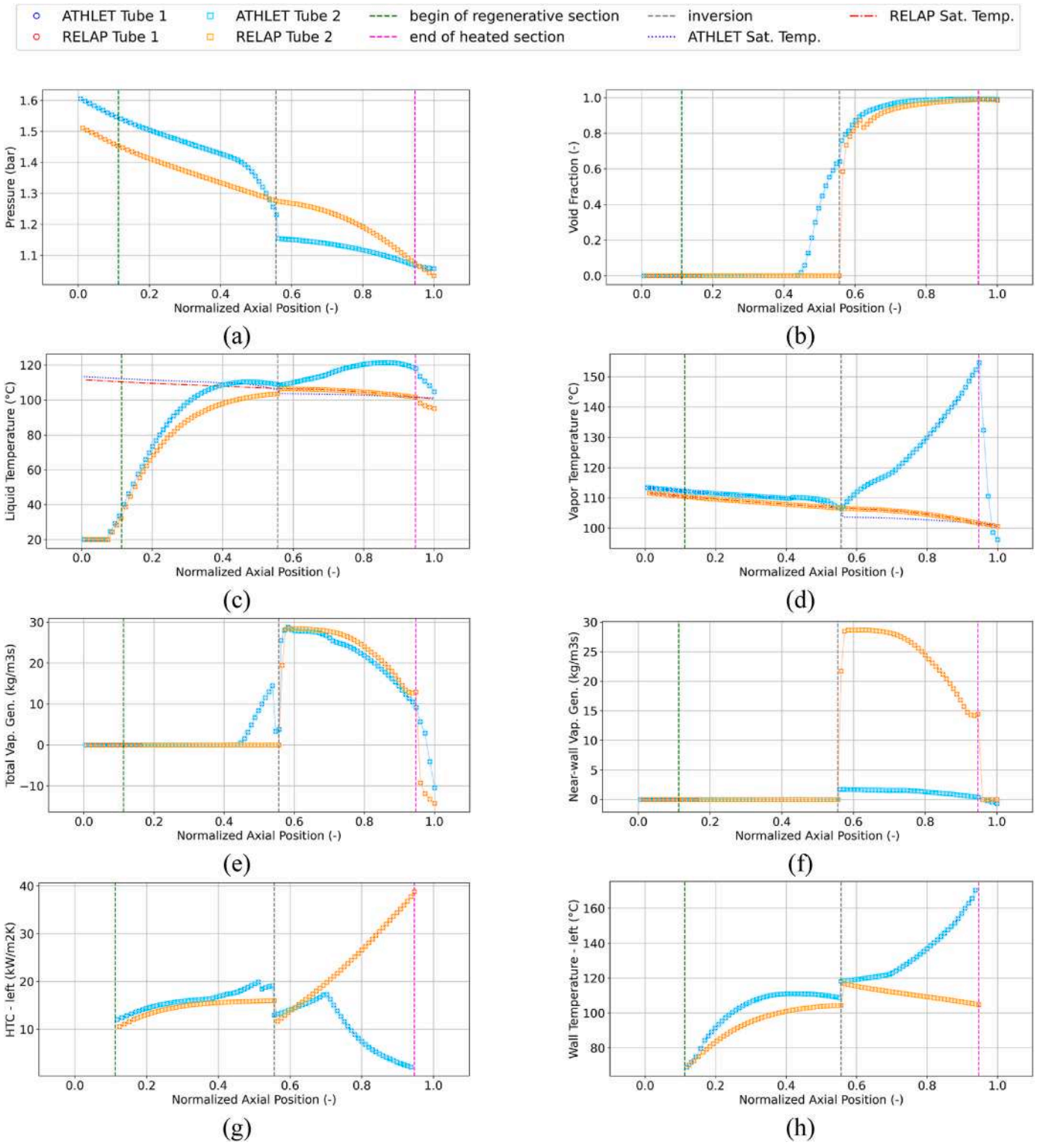


Fig. 6. Time-averaged distribution of the main quantities in both tubes (curves belonging to the same code may overlap) for a mass flow rate of 10 g/s (Case01). The standard deviation (although negligible compared to the marker size of the time-averaged value) is represented as bands of the corresponding tube color.

g., enthalpy quality, wall surface temperature, and void fraction) to determine the validity of each mode. However, ATHLET relies on numerical heat transfer modes in order to model a numerical blend between different boiling regimes.

These "blending" modes affect the distributions of the heat transfer coefficient (HTC) calculated on the left (or inner) side of the heat structures (in Figs. 6g and 7g). Specifically, ATHLET smooths the HTC transition in the proximity of the wall dryout using a cosine-shaped interpolation. Conversely, RELAP does not apply a gradual variation. Instead, the HTC calculated by RELAP increases to higher values before dropping abruptly in correspondence to the dryout. The location of the dryout is influenced by both the interphase model and the heat transfer modes. As can be seen in the distribution of the HTC and in the wall temperature (Fig. 7h), ATHLET predicts an earlier onset of the dryout,

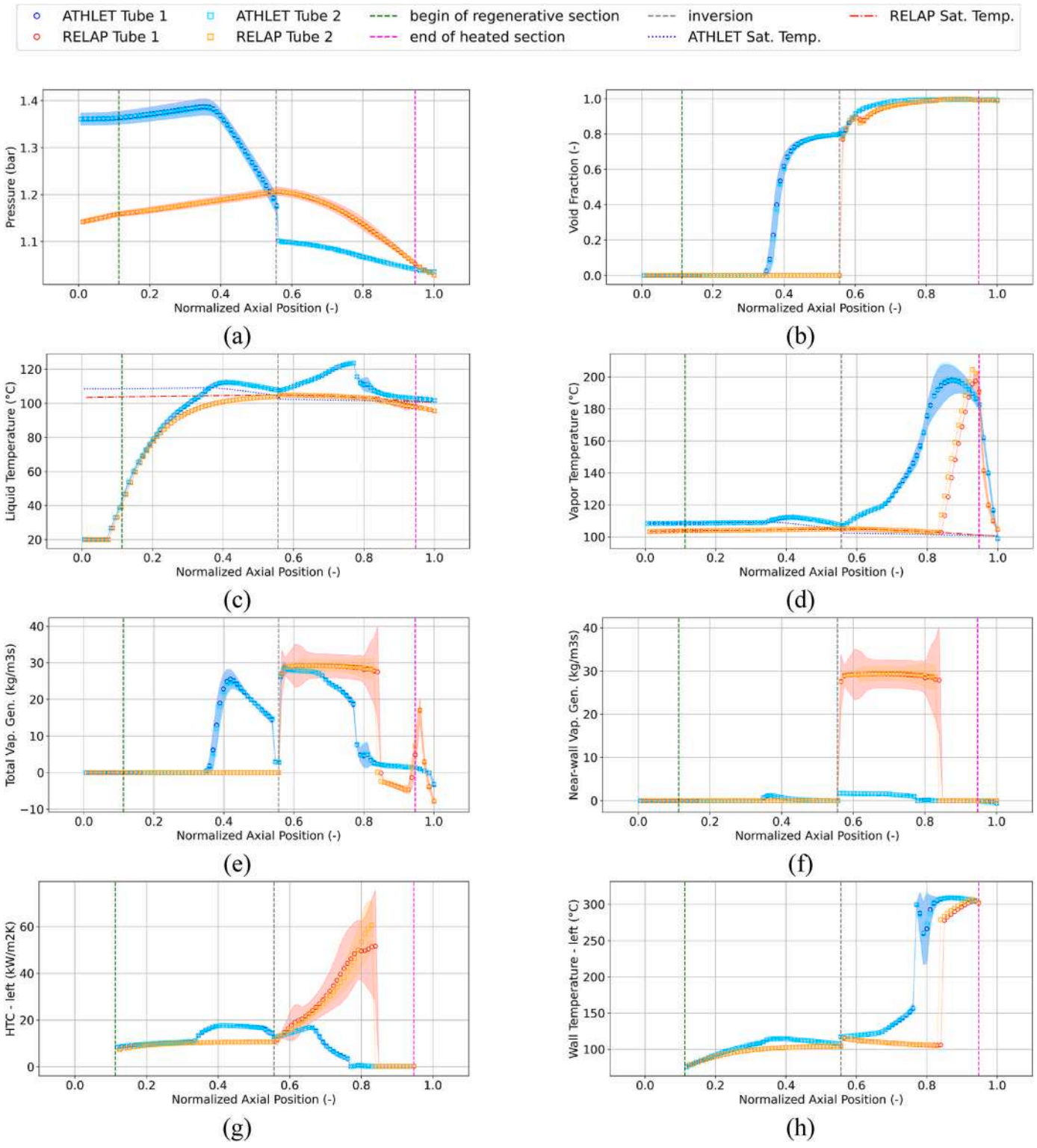


Fig. 7. Time-averaged distribution of the main quantities in both tubes (curves belonging to the same code may overlap) for a mass flow rate of 6 g/s (Case03). The standard deviation is represented as bands of the corresponding tube color.

which causes the wall temperature to increase. Such behavior is also observable for a mass flow rate of 10 g/s (Case01). Even if, for such mass flow, wall dryout condition is not fully achieved in both codes, Fig. 6g and h indicate the onset of the dryout predicted by ATHLET, as suggested by the decrease in the HTC and in the rise of the wall temperature.

As expected, tuning the ATHLET code parameters to disable the reduction of the evaporation rate and reduce the validity range of the blending heat transfer modes leads to an improved agreement between the codes, as shown in Fig. 8.

Namely, Fig. 8f displays better agreement in the near-wall evaporation rate with respect to Fig. 7f. Additionally, the HTC distribution predicted by ATHLET more closely resembles the distribution predicted by RELAP. However, major differences can still be observed, especially right before dryout. Nevertheless, the location of the dryout (observable

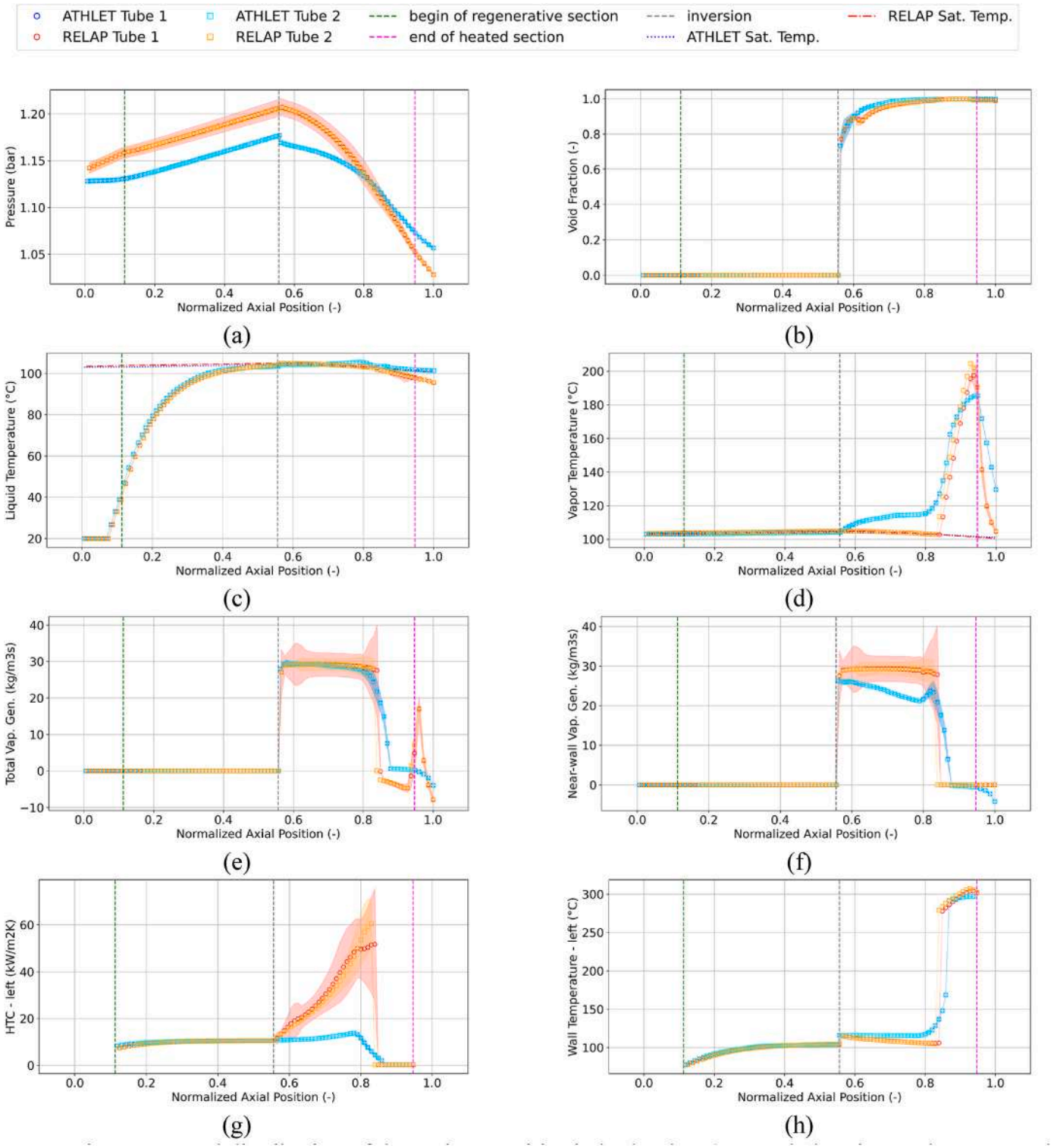


Fig. 8. Time-averaged distribution of the main quantities in both tubes (curves belonging to the same code may overlap) for a mass flow rate of 6 g/s (Case03). With respect to Fig. 7, ATHLET model is modified (disabled reduction of the evaporation rate and reduced validity range of the blending heat transfer modes). Standard deviation is represented as bands of the corresponding tube color.

especially in Fig. 8g and h) is more consistent between the codes. Such modifications in the ATHLET model improve also the agreement with the experimental results, as further discussed in the next section.

4.2. Code-to-experiment comparison

A preliminary comparison of the pre-test ATHLET and RELAP models, described in the previous section, is performed focusing on the cases listed in Table 3.

Three different experimental tests are considered, here referred to as Exp. 1, Exp. 2 and Exp. 3, and have been performed with a wall temperature setpoint of 350 °C. During these tests, the controlled mass flow rate has been changed using a stepwise approach in the range between 3.5 g/s and 10 g/s. The experimental results, presented with time-

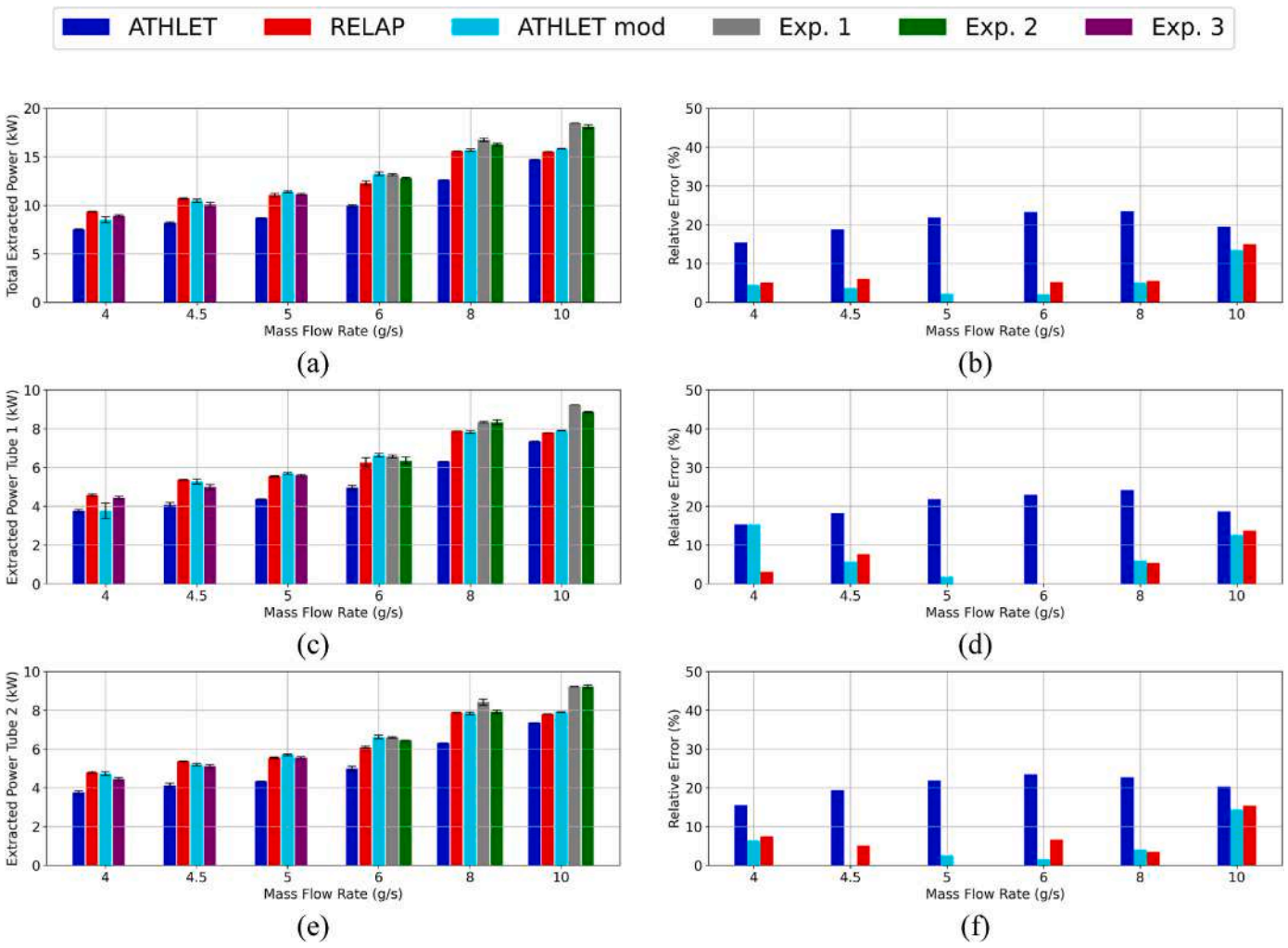


Fig. 9. Comparison of the power extracted by the test section (a), and by each tube individually (c) and (e). The standard deviation is represented by a black error bar. The relative error between the numerical and experimental results is reported for the entire test section (b), and for each tube (d) and (f).

averaged values and standard deviations, are obtained once steady-state conditions are achieved for each mass flow rate. During Exp. 1 the feedwater mass flow rate has been decreased starting from 10 g/s, whereas during Exp. 2 the mass flow rate has been increased starting from 3.5 g/s. During Exp. 3 the mass flow rate has been decreased starting from 5 g/s with a finer step. As mentioned, the experimental results concerning 3.5 g/s are excluded from this study due to the onset of an unstable behavior of the test section, which is currently out of the

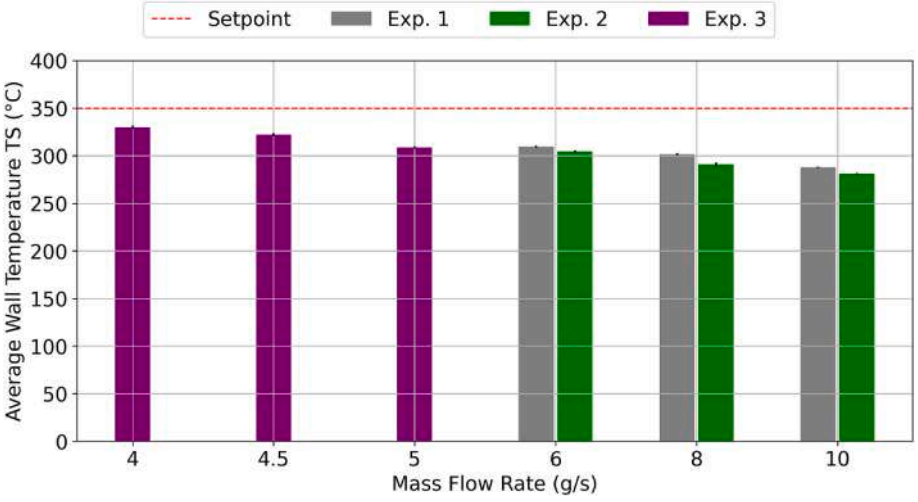


Fig. 10. Representation of the average (measured) wall temperature of the test section as a function of the mass flow rate. The standard deviation is represented by a black error bar (although almost negligible in some cases).

scope of the comparison.

Fig. 9 shows a good agreement between the experimental data and the code results, except for the ATHLET results calculated with the unmodified near-wall evaporation model and heat transfer mode selection. Specifically, the relative error (in Fig. 9b, d, and 9f) of the default AHTLET model reaches 20% as the mass flow rate increases. Conversely, the relative error of the RELAP and modified ATHLET models remains below 10%, except for the mass flow rate of 10 g/s, for which all errors remain below 20%.

Such discrepancy can be attributed to the modelling approach implemented in the pre-test models which is not fully representative of the DCI Test Facility.

In fact, Fig. 10 shows that the facility is unable to reach the wall temperature setpoint at high mass flow rates, particularly in the lower section of the tubes. In contrast, in the simulations the wall temperature is imposed as a boundary condition and is therefore inherently achieved.

Fig. 11 compares the power supplied by each electrical heater in the experimental setup with the power delivered by the corresponding heat structure in the computational models. The first heater is located at the bottom of the bayonet tube. The results indicate that, for all three cases, the experimental power supplied to the lower section of the bayonet tube is approximately 20% higher than that in the numerical simulations.

Consequently, Figs. 10 and 11 suggest that the main issue is a

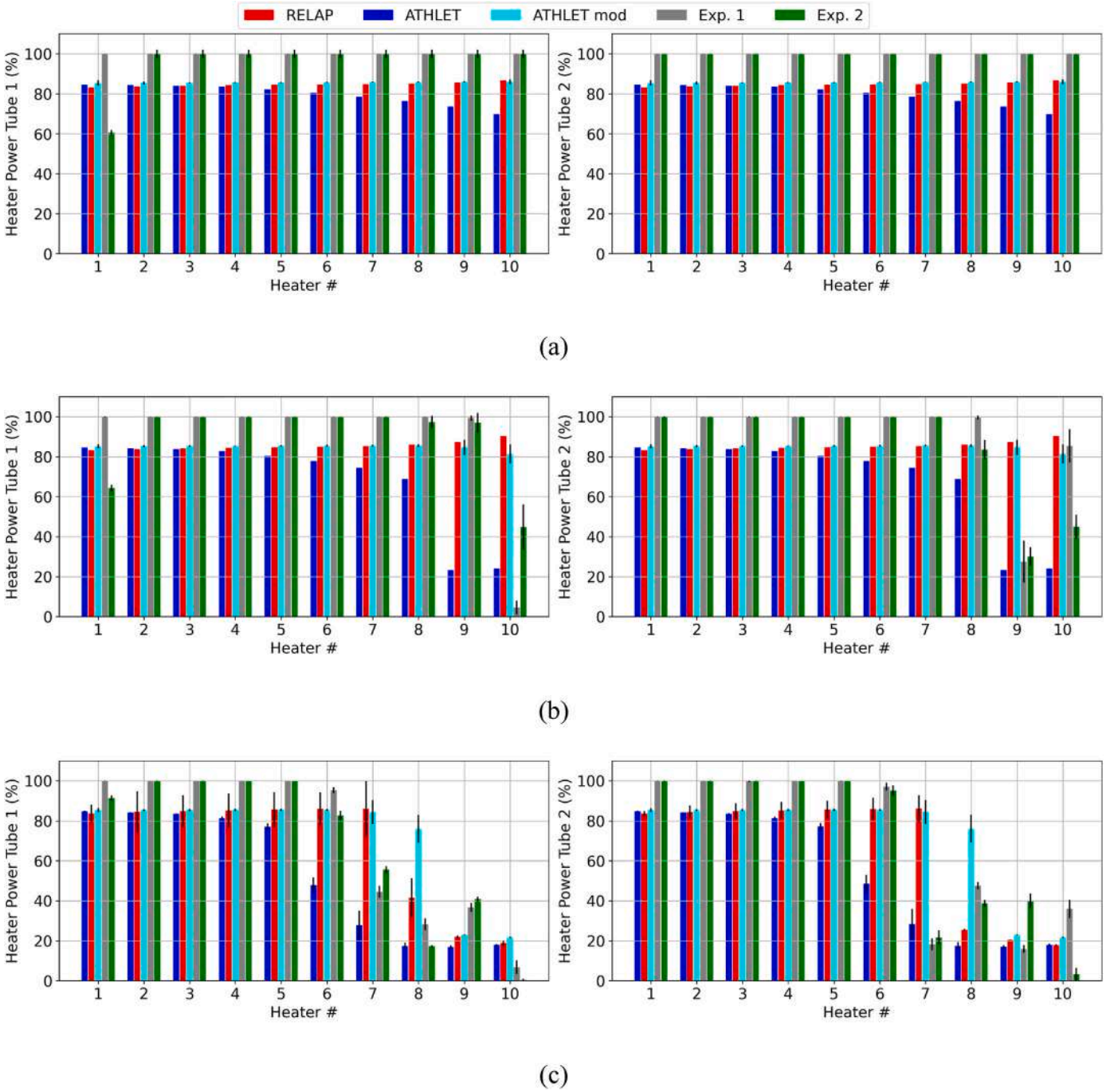


Fig. 11. Comparison of the power distribution in correspondence of each electrical heater for three different mass flow rates: (a) 10 g/s or Case01, (b) 8 g/s or Case02, and (c) 6 g/s or Case03. The standard deviation is represented by a black error bar. Power percentages refer to the nominal power of a single electrical heater. Heater 1 is located at the bottom of the tube.

discrepancy in the overall thermal resistance of the tubes. In fact, while the wall temperature is prescribed in the simulations, the numerical power remains generally below the nominal value (100% value in Fig. 11).

In particular, the higher experimental power supplied to the bottom of the tubes might suggest a lower effective thermal resistance of the helium gap in the experimental setup with respect to the one computed in the simulations. The possible reasons may be associated to the presence of metallic spacers within the helium gap, which contribute to reduce the effective thermal resistance of the tubes. Additionally, deviations of the helium gap from its nominal value (potentially arising from manufacturing or assembly processes and not easily inspectable) may contribute to increase the thermal conductivity.

To quantify the influence on the numerical results of helium gap conductivity among other influential parameters, a preliminary uncertainty quantification analysis is performed using the ATHLET code, and is discussed in the following section.

Finally, the power distribution provides useful insight into the prediction of the dryout location. Both the RELAP and the modified ATHLET models predict a delayed onset of the dryout, whereas the unmodified ATHLET model generally predicts an earlier onset of the dryout.

4.3. Preliminary uncertainty quantification analysis

To improve the agreement of the numerical results obtained with the ATHLET code with both the RELAP code and the experiments, it has been necessary to adopt a different modelling approach, especially concerning the interphase heat transfer model and the heat transfer mode selection. To assess if the achieved level of agreement with the experiments can be further improved, and to determine the influence of the thermal conductivity of the helium gap and of the wall temperature, a preliminary uncertainty quantification (UQ) analysis has been carried out taking as reference the modified ATHLET model (with disabled reduction of the near-wall evaporation and reduced validity of the blending heat transfer modes) for a mass flow rate of 6 g/s (Case03). This case has been selected due to the presence of the dryout, while being also sufficiently far from a possible unstable behavior of the test section.

The perturbed parameters, listed in Table 4, are selected from a subset of those presented in Ref. [19], as well as based on engineering judgment for the application considered in this work. Namely, the parameters involved in the analysis are those affecting the validity of the blending heat transfer mode between the nucleate boiling and the film boiling regimes, the dryout and post-dryout regime, the evaporation rate (at low pressure), the helium conductivity, and the wall temperature boundary condition. The perturbation ranges have been chosen based on the authors' engineering judgment.

Table 4
List of the perturbed parameters.

Name	Description	Reference Value	Distribution	(Min, Max)
ohwnb	Nucleate Boiling HTC Multiplier	1.0	Normal	(0.8, 1.2)
ohwfb	Film Boiling HTC Multiplier	1.0	Normal	(0.65, 1.3)
ohvfc	Forced Convection (vapor) HTC Multiplier	1.0	Normal	(0.85, 1.25)
otmfb	Minimum Film Boiling Temperature Multiplier	1.0	Normal	(0.2, 1.8)
otrnb	Minimum Critical Heat Flux Multiplier	1.0	Normal	(0.2, 1.8)
oaddi	Evaporation Rate at low pressure Multiplier	0.2	Uniform	(0.1, 0.5)
pol11	Minimum Void Fraction for the validity of the blending heat transfer mode between nucleate and film boiling	0.995	Uniform	(0.967, 0.998)
cond_mul	Multiplier of the thermal conductivity of the helium gap	1.0	Uniform	(0.5, 3.0)
temp_mul	Multiplier of the wall temperature boundary condition	1.0	Uniform	(0.8. 1.1)

A total of 93 simulations (according to the one-sided second order Wilks' formula [20]) of the UQ set have been run using a Monte Carlo method, which simultaneously assigns random samples inside the given probability distribution to each parameter.

Fig. 12a shows the evolution of the power extracted by the test section for each simulation. Overall, the computed power lies in a range between approximately 6.0 kW and 20 kW. In addition, Fig. 12b reports the probability density of the extracted power and highlights how the peak lies between 12 kW and 14 kW and encompasses the experimental values.

Finally, Fig. 12c reports the quantification of the influence of each parameter on the extracted power with the partial correlation coefficients (PCCs). PCCs can be used as a measure of the influence of a parameter on the extracted power, once the influences from all other parameters are eliminated. The higher the value of a PCC, the greater the influence of the parameter on the extracted power. From the plot, it can be observed that, as expected, the thermal conductivity multiplier (cond_mul) and the wall temperature multiplier (temp_mul) exert the highest influence on the computation of the extracted power. Future work will focus on post-test analyses that will encompass a comprehensive evaluation of the effective thermal conductivity of the helium gap as well as the implementation of the heater PID control logic to better reproduce the behavior of the test section.

5. Conclusions

A code-to-code benchmark has been performed taking advantage of the pre-test analysis of the DCI Test Facility, carried out with the system thermal-hydraulic codes AC^2-ATHLET 3.4.1 and RELAP/SCDAPSIM/MOD4.1.

The comparison between the time-averaged results points towards two main sources of discrepancy: one in the methodology used for determining the heat transfer mode, and the other in the near-wall evaporation implemented in the heat and mass transfer model.

The preliminary comparison with the experimental results has been focused on the extracted power and on the power distribution. A good agreement in the power extracted by the test section has been observed for the proposed RELAP model and for the modified ATHLET model (namely with disabled reduction of the near-wall evaporation model and reduced validity of the blending heat transfer mode). Specifically, the discrepancy from the experiments decreases as the mass flow rate decreases. At high mass flow rates, the numerical models are not capable of fully reproducing the behavior of the facility, namely the reduction of the average wall temperature as observed in the experiments.

The comparison of the power distribution highlights the capability of the codes to predict the onset of the dryout. Overall, the RELAP model and the modified ATHLET model predict a delayed onset of the dryout as compared to the experimental findings. Such difference could be due to the higher effective thermal conductivity of the helium gap in the experimental facility.

A preliminary uncertainty quantification analysis performed with the modified ATHLET model seems to endorse the latter hypothesis. Future work will focus on a more comprehensive uncertainty propagation analysis, including also the proposed RELAP model. Additional efforts will be centered on the determination of the effective thermal conductivity of the helium gap thanks to a more accurate model of the facility, which will include the PID logic determining the power supplied by each heater. In fact, post-test upgrades will be implemented in the model to improve the comparison with the full set of experimental cases

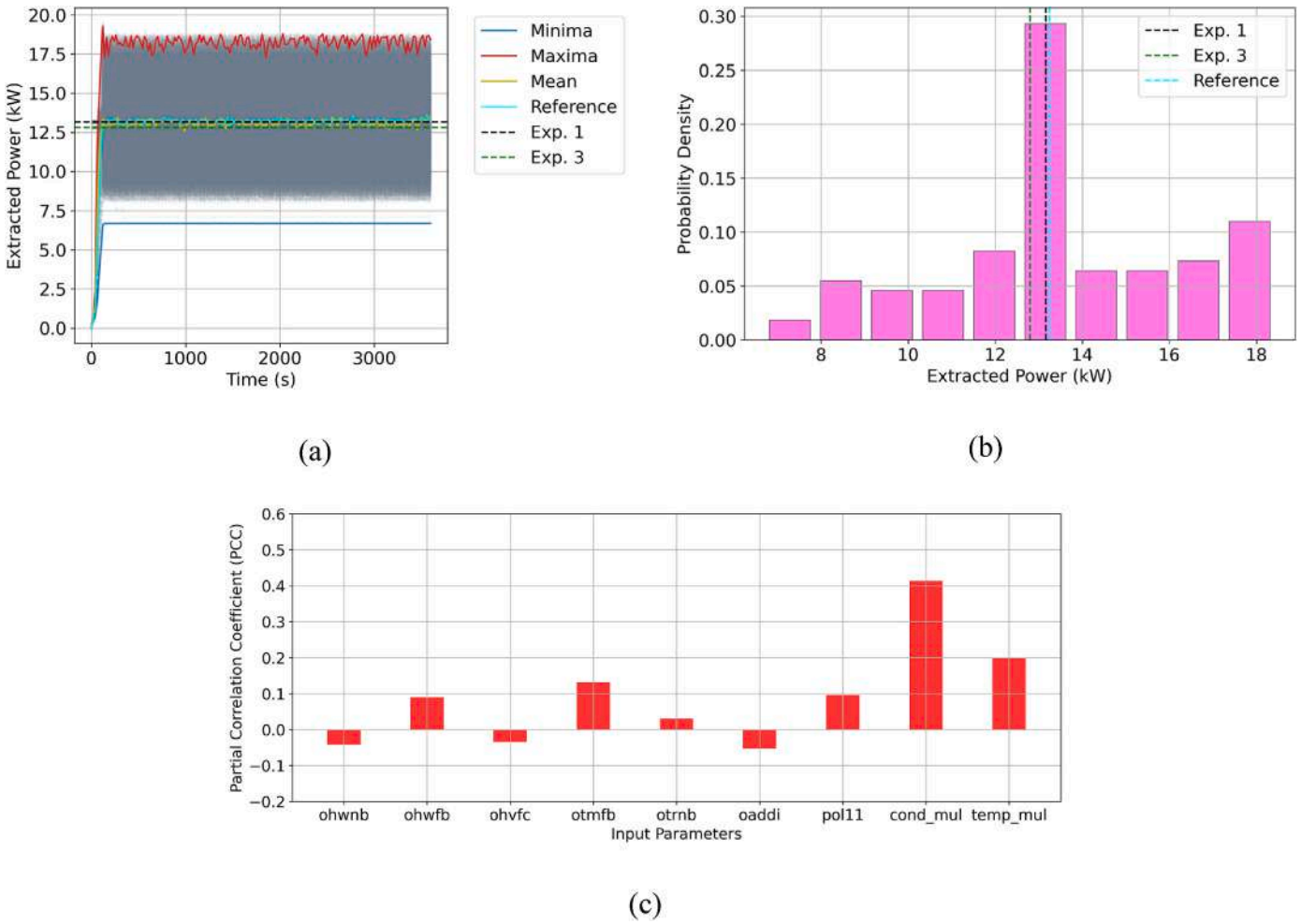


Fig. 12. (a) Evolution of the extracted power for the 93 simulations (in grey); (b) Probability density of the extracted power; (c) representation of the Partial Correlation Coefficients relative to the power extracted.

and measurements, taking also into account the onset of two-phase flow instabilities.

CRediT authorship contribution statement

Danilo Caterino: Writing – review & editing, Writing – original draft, Methodology, Investigation, Data curation. **Giuseppe Spina:** Writing – review & editing, Supervision, Methodology, Data curation. **Roberto Bonifetto:** Writing – review & editing, Supervision, Investigation. **Antonino Lombardo:** Writing – review & editing, Software, Methodology. **Fabio Moretti:** Writing – review & editing, Supervision, Project administration, Conceptualization. **Giuseppe Francesco Nallo:** Writing – review & editing, Supervision, Conceptualization. **Valeria Parrinello:** Writing – review & editing, Conceptualization. **Matteo Rostagno:** Data curation. **Raffaella Testoni:** Writing – review & editing, Supervision, Investigation.

Declaration of competing interest

The authors declare that they have no known competing financial interests or personal relationships that could have appeared to influence the work reported in this paper.

Acknowledgments

All activities described in this work pertain to the corresponding author's PhD scholarship, carried out at Politecnico di Torino and funded by *new*cleo SpA and the Italian Ministry of Education through the PNRR founds.

Appendix A. – Nodalization analysis

The nodalization analysis has been focused on increasing the number of volumes used for the discretization of the heated length of each tube. Namely, 40, 60, and 80 vol have been simulated. Focusing on a single case (i.e., 8 g/s or Case02), Fig. 13 shows that the total extracted power is not significantly affected by the number of volumes. Fig. 14 shows instead that the extent of the numerical oscillations (represented by a black error bar) increases as the number of volumes increases, especially in RELAP (Fig. 14a). To limit the numerical oscillations and to minimize the required elapsed time, 40 vol are used in the simulations presented in this work. Whereas future work will address more thoroughly the causes of the observed oscillations.

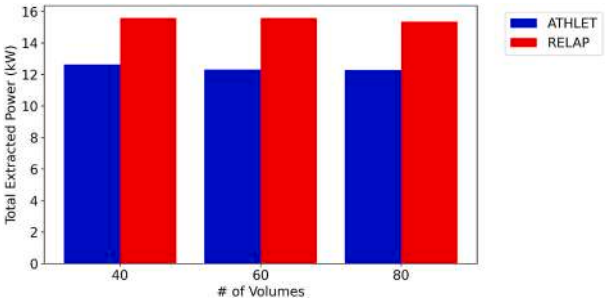


Fig. 13. Power extracted by the test section for different number of volumes used to discretize the heated length.

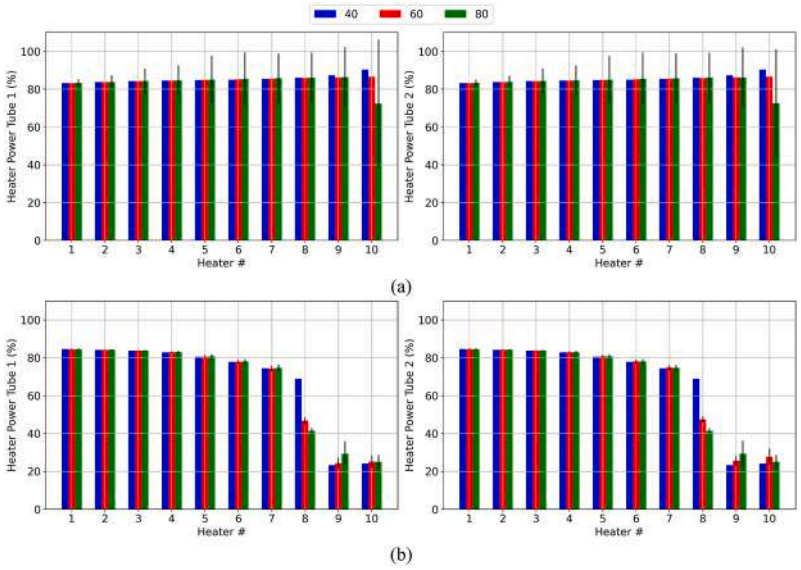


Fig. 14. Power distribution in correspondence of each experimental heater for increasing number of volumes used to discretize the heated length in RELAP (a) and ATHLET (b).

References

[1] C. Smith, Lead-Cooled Fast Reactor (LFR) design: safety, neutronics, thermal hydraulics, structural mechanics. Fuel, Core, and Plant Design, Lawrence Livermore National Lab.(LLNL), Livermore, CA (United States), 2010.

[2] C.F. Smith, L. Cinotti, Lead-cooled fast reactor, in: Handbook of Generation IV Nuclear Reactors, Elsevier, 2019, pp. 119–155.

[3] P. Lorusso, S. Bassini, A. Del Nevo, I. Di Piazza, F. Giannetti, M. Tarantino, M. Utili, GEN-IV LFR development: status & perspectives, Prog. Nucl. Energy 105 (2018) 318–331.

[4] newcleo, Newcleo official website [Online]. Available: https://www.newcleo.com/. (Accessed 9 January 2026).

[5] A. Alemberti, D. De Bruyn, G. Grasso, L. Mansani, D. Mattioli, F. Roelofs, others, The European lead fast reactor strategy and the roadmap for the demonstrator ALFRED, in: International Conference on Fast Reactors and Related Fuel Cycles: Safe Technologies and Sustainable Scenarios (FR13), 2013. Paris, France.

[6] L. Damiani, A.P. Prato, Simulation model of a passive decay heat removal system for lead-cooled fast reactors, J. Eng. Gas Turbines Power 137 (2014) 742–4795.

[7] F. Di Maio, N. Pedroni, B. Toth, L. Burgazzi, E. Zio, Reliability assessment of passive safety systems for nuclear energy applications: state-of-the-art and open issues, Energies 14 (2021) 4688.

[8] L.C. Ruspini, C.P. Marcel, A. Clausse, Two-phase flow instabilities: a review, Int. J. Heat Mass Tran. 71 (2014) 521–548.

[9] C. Bertani, N. Falcone, A. Bersano, A. Azzarone, M. De Salve, B. Panella, Experimental study of a natural circulation loop and RELAP5-3D analysis, in: Journal of Physics: Conference Series, 2020.

[10] R. Marinari, M. Tarantino, F. Nitti, A. Alemberti, M. Caramello, A. Achilli, R. Ferri, E. Rizzo, F. Giannetti, SIRIO: an experimental facility for a new heat removal system passively controlled by non-condensable gases, in: International Conference on Nuclear Engineering, 2018.

[11] K. Van Tichelen, G. Kennedy, F. Mirelli, A. Marino, A. Toti, D. Rozzia, E. Cascioli, S. Keijers, P. Planquart, Advanced liquid-metal thermal-hydraulic research for MYRRHA, Nucl. Technol. 206 (2020) 150–163.

[12] P. Lorusso, A. Pesetti, M. Tarantino, V. Narcisi, F. Giannetti, N. Forgione, A. Del Nevo, Experimental analysis of stationary and transient scenarios of alfred steam generator bayonet tube in circe-hero facility, Nucl. Eng. Des. 352 (2019) 110169.

[13] M. Polidori, Deliverable 2.2: Description of HERO-2 Facility and Simulations, 2022.

[14] P. Schöffel, A. Di Nora, D. Eckert, J. Markus, D. von der Cron, F. Weyermann, A. Wielenberg, *AC2-ATHLET 3.4.1 Code Manual,* Gesellschaft für Anlagen- und Reaktorsicherheit (GRS), 2023.

[15] L.J. Siefken, E.W. Coryell, E.A. Harvego, J.K. Hohorst, *SCDAP/RELAP5/MOD 3.3 Code Manual,* Idaho National Engineering and Environmental Laboratory, 2001.

[16] A. Barbenesi, J.-S. Genot, S. Nardi, M. Tarantino, In-Service inspection & repair strategy for newcleo Lead-cooled fast reactor, e-J. Nondestruct. Test. (2023).

[17] F. Dittus, L. Boelter, Heat transfer in automobile radiators of the tubular type, Int. Commun. Heat Mass Tran. 12 (1985) 3–22.

[18] J.C. Chen, Correlation for boiling heat transfer to saturated fluids in convective flow, Ind. Eng. Chem. Process Des. Dev. 5 (1966) 322–329.

[19] Post-BEMUSE Reflood Model Input Uncertainty Methods (PREMIUM) Benchmark - Final Report, Nuclear Energy Agency Commitee On The Safety of Nuclear Installations, 2017.

[20] B.T. Hallee, K.G. Metzroth, Evaluation of Wilks' one-sided Non-parametric Formula Against Analytical Parametric Methods, 2017.